Separation Science and Technology
Publication details, including instructions for authors and subscription information:
http://www.informaworld.com/smpp/title~content=t713708471

Computational Modeling of Ionic Transport in Continuous and Batch Electrodialysis

Paula Moon[a]; Giselle Sandí[b]; Deborah Stevens[a]; Riza Kizilel[c]
[a] Mathematics and Computer Science, Argonne National Laboratory, Argonne, Illinois, USA [b] Chemistry Division, Argonne National Laboratory, Argonne, Illinois, USA [c] Department of Chemical and Environmental Engineering, Illinois Institute of Technology, Chicago, Illinois, USA

Online publication date: 08 July 2010

To cite this Article Moon, Paula , Sandí, Giselle , Stevens, Deborah and Kizilel, Riza(2004) 'Computational Modeling of Ionic Transport in Continuous and Batch Electrodialysis', Separation Science and Technology, 39: 11, 2531 — 2555
To link to this Article: DOI: 10.1081/SS-200026714
URL: http://dx.doi.org/10.1081/SS-200026714

SEPARATION SCIENCE AND TECHNOLOGY
Vol. 39, No. 11, pp. 2531–2555, 2004

Computational Modeling of Ionic Transport in Continuous and Batch Electrodialysis[#]

Paula Moon,[1,*] Giselle Sandí,[2] Deborah Stevens,[1] and Riza Kizilel[3]

[1]Mathematics and Computer Science and [2]Chemistry Division, Argonne National Laboratory, Argonne, Illinois, USA
[3]Department of Chemical and Environmental Engineering, Illinois Institute of Technology, Chicago, Illinois, USA

ABSTRACT

We describe the transport of ions and dissociation of a single salt and a solvent solution in an electrodialysis (ED) stack. An ED stack basic unit is made of a two-compartment cell: dilute and concentrate. We use the fundamental principles of electrochemistry, transport phenomena, and

---

*Correspondence: Paula Moon, Argonne National Laboratory, 9700 South Cass Ave., Argonne, IL 60439, USA; Fax: (630) 252-9281; E-mail: pmoon@anl.gov.

DOI: 10.1081/SS-200026714 0149-6395 (Print); 1520-5754 (Online)
Published by Marcel Dekker, Inc. www.dekker.com

thermodynamics to describe mechanisms and to predict the performance of the ED process. We propose and analyze three model formulations for a single salt (KCl). The first and the second models are for a one- and two-dimensional continuous ED, and the third examines batch ED. The models include the effect of the superficial velocity in the boundary layer near the ion-exchange membranes. We examine the diffusion and electromigration of ions in the polarization region and consider electromigration and convection in the bulk region. We show that the ionic surface concentration of both membranes in the dilute compartment is affected by two parameters: flow rate and current density. We also show that in the dilute compartment, concentration changes along the *x*-axis are greater than along the *y*-axis because the ionic flux along the *x*-axis is greater and is in the direction of the current. In simulations where the KCl dilute concentration ranges from 200 to 500 $\mathrm{mol\,m^{-3}}$ with a constant concentrate concentration, the dilute voltage drop accounts for more than 36% of the total voltage drop. This value is reduced to 7% as the dilute concentration increases and contributions of both ion-exchange membrane drops account for more than 50% of the total cell voltage drop. All the three models were validated experimentally.

Key Words: Electrochemical modeling; Electrodialysis; Membrane; Electrochemical separation; Ionic solution.

INTRODUCTION

Electrodialysis (ED) is an electrochemical process used for removing ions in an aqueous solution. The application of an electrical potential difference between two electrodes in contact with membranes and an aqueous ionic solution generates an electric field. The electric field creates the basis for the migration of ions across ion-exchange membranes. The basic ED unit is a two-compartment cell, with dilute and concentrate compartments side by side.

The ion-exchange membranes used in ED are thin, uniform sheets containing a fixed charge.[1] The fixed charges attached to the polymer chains of the membranes reject ions of the same charge (co-ions).[2] As a result, the membrane maintains a relatively high concentration of counter ions. These counter ions carry most of the electric current through the (anion-exchange or cation-exchange) membrane. The transport of counter ions occurs by diffusion and by migration between the membrane and the surrounding solution.

The objective of this work is to understand and predict the transport mechanisms of potassium chloride through ion-exchange membranes with potential used in ED. Computer simulations of transport of potassium chloride

across ion-exchange membranes provide information on the behavior of ion transport at the molecular level and for batch process.

In the present paper, the electrochemical transport phenomena of the ion-exchange membranes were developed. The potassium chloride concentration in the membrane was determined at any given position by a set of electrochemical parameters determined experimentally or found in the literature. On the other hand, electrochemical models, which were studied in detail by considering the concentration profile, superficial velocity, voltage, and current distribution, were applied to the study of continuous and batch ED.

A schematic illustration in Fig. 1 shows some of the ion fluxes present in a cation-exchange membrane located between a dilute and a concentrate compartment. In reality, flow is three-dimensional (3-D) but can be approximated as 2-D for modeling purposes. The solution being processed flows along the *y*-axis and is perpendicular to a direct electrical potential (*x*-axis).

THEORETICAL CONSIDERATIONS

The following assumptions were made for the ED model: (1) quasi-steady state; (2) concentration-independent diffusion coefficients, mobility, and transport number; (3) complete dissociation of ions; (4) average boundary layer thickness; (5) uniform flow distribution away from the boundary layers (in the bulk fluids); (6) ideal membranes (100% exclusion of co-ions in both ion-exchange membranes types); (7) incompressible fluid; (8) negligible diffusion and migration (based on the *Pe* number, 8.0×10^6) along the direction of the bulk flow in comparison with convective transport in the solution phase; (9) negligible convective transport in the direction perpendicular to the membranes in comparison with diffusion and migration in the solution phase; and (10) identical voltage drop for each cell pair.

Model Around the Membranes

The Nernst–Planck equation is the basis for characterizing ion transport in the solution phase:[3–7]

$$J_i = -n_i u_i C_i F \nabla\Theta - D_i \nabla C_i + C_i v \tag{1}$$

The subscript i refers to species i; J_i, the flux of species i; n_i, the valence of species i; u_i, the mobility of species i; C_i, the concentration of species i; $\nabla\Theta$, the potential difference; D_i, the diffusion coefficient of species i; F, the Faraday constant; and v, the fluid velocity.

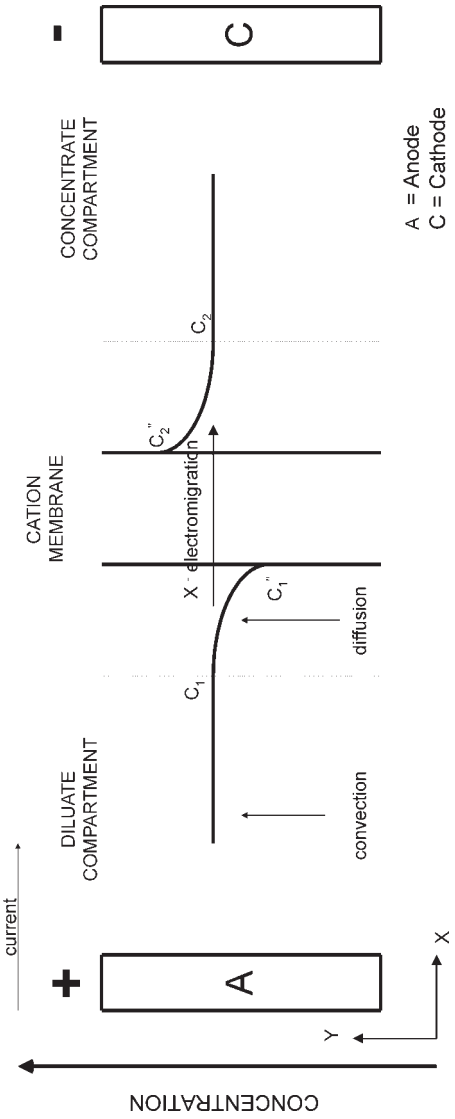

Figure 1. Schematic illustration of transport mechanisms near a cation-exchange membrane.

The first, second, and third terms in Eq. (1) represent gradients in potential, concentration, and momentum, resulting in electromigration, diffusion, and convection, respectively.[8]

Membrane Phase Mass Transport

We first consider the membrane phase mass transport. We use the KCl (salt) and water (solvent) system as an example. For the single salt under study, the ionic species are K^+ and Cl^-. The mass flux of each ion in the membrane, $\bar{J}_i$, is also represented by the Nernst–Planck equation, as follows:[2,9]

$$\bar{J}_i = -\bar{D}_i\left(\frac{d\bar{C}_i}{dx} + n_i\frac{\bar{C}_i F}{RT}\frac{d\bar{\Theta}}{dx}\right) \tag{2}$$

Subscripts $i = 1, 2$ refer, respectively, to K^+ and Cl^-; $\bar{D}_i$, the diffusion coefficient of species i in the membrane; and $\bar{C}_i$ and $\bar{\Theta}$, the concentrations of species i and the potential in the membrane, respectively.

Because of the electrostatic repulsion of co-ions by the fixed-charge group, only the counter ions absorb onto the fixed-charge sites. Counter ions migrate through a membrane when a potential gradient is applied and are freely exchanged at these fixed-charge sites. We assume that each absorbed counter ion is attached to an individual fixed-charge site. The concentrations of fixed-charge sites and absorbed counter ions adjust so that any small-volume element of membrane remains electrically neutral:[5,10]

$$\sum |n_i|\bar{C}_i = Q_{\mathrm{AM}} \quad \text{or} \quad Q_{\mathrm{CM}} \tag{3}$$

Q_{AM} and Q_{CM} refer to the capacities of anion- and cation-exchange membranes. For the single salt under study, each ion-exchange membrane type has only one counter ion. The capacity of each ion-exchange membrane is a known value. The current density, $\bar{I}$, in the membrane is defined as:

$$\sum n_i\bar{J}_i = \frac{\bar{I}}{F}, \quad \text{in a single salt } n_i\bar{J}_i = \frac{\bar{I}}{F} \tag{4}$$

Based on the above assumptions, $d\,\bar{C}/dx = 0$ and reformulating Eq. (2) gives the linear voltage drop, $d\,\bar{\Theta}/dx$, in the cation- and the anion-exchange membranes:

$$\frac{d\bar{\Theta}^{\text{CM or AM}}}{dx} = -\frac{RT\bar{I}}{n_i^2F^2\bar{D}_i\bar{C}_i}, \quad i = 1, 2 \tag{5}$$

Dilute and Concentrate Solution Phase Transport Along the *x*-Axis (1-D Continuous Model)

Consider the mass flux of species i in either the dilute or the concentrate boundary layers through a section of thickness Δx, width W, and height L, as shown in Fig. 2.

A material balance for a transporting ion i in the boundary layer is written as:

$$\frac{\partial C_i}{\partial t} + \frac{\partial J_i}{\partial x} = R_i \tag{6}$$

where R_i is the production rate of ion i by chemical reaction. Assuming that the dissociation reaction of the single salt occurs instantaneously, the production term is zero. Concentration in a solution changes so little in each pass through a cell that a quasi-steady state can be assumed.[6] Therefore, the accumulation term in Eq. (6) is also zero.

The boundary layer ionic transport equation can then be expressed as:

$$\frac{\partial J_i}{\partial x} = 0 \tag{7}$$

We solve for a cell pair that consists of a dilute compartment and a concentrate compartment. The fluid flow forms boundary layers near each membrane. As shown in Fig. 1, the solution flows upward (y-axis) in a compartment and perpendicular to a direct electric potential (x-axis).

In a typical ED stack, a mesh or inert promoter of 0.76-mm thickness is introduced between the individual membrane sheets to support the membrane and to help control the feed solution flow distribution. This mesh provides the maximum mixing of the solutions at the membrane surfaces[2] and increases eddy transport of momentum and mass.[11] It is assumed that there will be no significant fluid flow in the x-direction because the stack employs the sheet-flow principle, where the solution flows parallel to the membrane to improve the contact time between the solution and the membrane.[2] The presence of a mesh in an ED compartment increases the mass transfer coefficient by a factor of 2–7. A correlation of the mass transfer coefficient k_L, using a mesh similar to that used in the ED stack, is given by Goodridge and Scott:[11]

$$k_L = 1.25 \frac{D_s}{d_e} Re^{0.46} Sc^{1/3} \quad (150 < Re < 1500) \tag{8}$$

where D_s is the salt solution diffusion coefficient, and d_e is the hydraulic diameter.

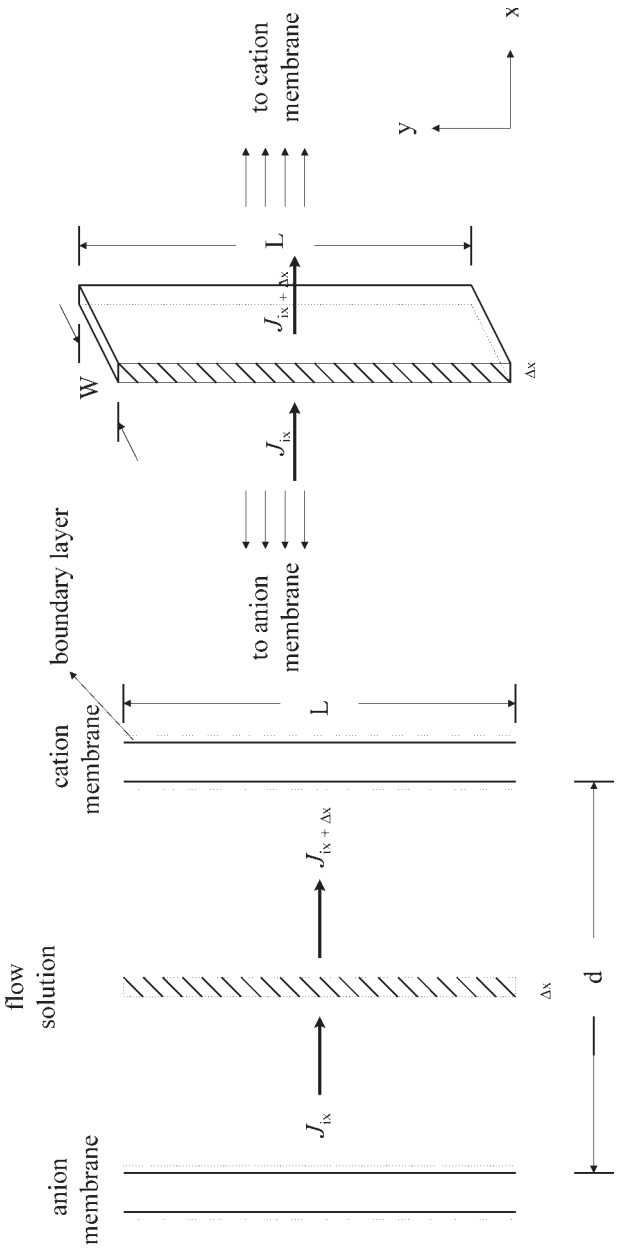

Figure 2. One-dimensional material balance in the flow solution around the membranes.

Therefore, in the boundary layers, mass transfer due to diffusion and electromigration dominates. In the bulk solution, there is no concentration gradient along the *x*-axis, and the ionic species move only by electromigration. Thus, combining Eq. (1) and the one-dimensional material-balance, Eq. (7) yields:

$$-D_i \frac{\partial^2}{\partial x^2}(C_{h,i}) - \frac{\partial}{\partial x}\left[(n_i D_i C_{h,i})\frac{F}{RT}\frac{\partial \Theta}{\partial x}\right] = 0 \tag{9}$$

where the subscript h refers to either the dilute or the concentrate compartment. We use the Nernst–Einstein relationship[12] for ion transport in dilute systems. This allows for the elimination of the ionic mobility, u_i, as an independent parameter (i.e., $u_i = D_i/RT$).

Since the flow of charge is related to the current density I ($\mathrm{A\,m^{-2}}$) in solution,

$$I = F\sum_i n_i J_i \tag{10}$$

Rearranging Eq. (10) for each species, ion-exchange compartment, and for

$$J_i = D\frac{\partial(C_{h,i})}{\partial x} - \left[(n_i D_i C_{h,i})\frac{F}{RT}\frac{\partial \Theta}{\partial x}\right],$$

we can write the following for the electrical potential:

$$\frac{\partial \Theta}{\partial x} = -\left(\frac{I/F + \sum_{i=1}^{2} n_i D_i(\partial C_{h,i}/\partial x)}{\sum_{i=1}^{2} n_i^2 D_i C_{h,i}}\right)\frac{RT}{F} \tag{11}$$

To solve the differential Eq. (9) for species i and compartments h (C_i, h), we must specify the initial and the boundary conditions. We use the electroneutrality condition to decrease the total number of material-balance equations to be solved. The variable x represents the distance coordinate in a cell pair: x ranges from P1 = 0 in Region I to P8 in Region VII, as indicated in Fig. 3.

We divide each cell pair of the ED stack into seven regions, as follows: Region I, boundary layer near anion membrane on the concentrate side; Region II, anion membrane; Region III, boundary layer near anion membrane on the dilute side; Region IV, dilute bulk region; Region V, boundary layer near cation membrane on the dilute side; Region VI, cation membrane; Region VII, boundary layer near cation concentrate side.

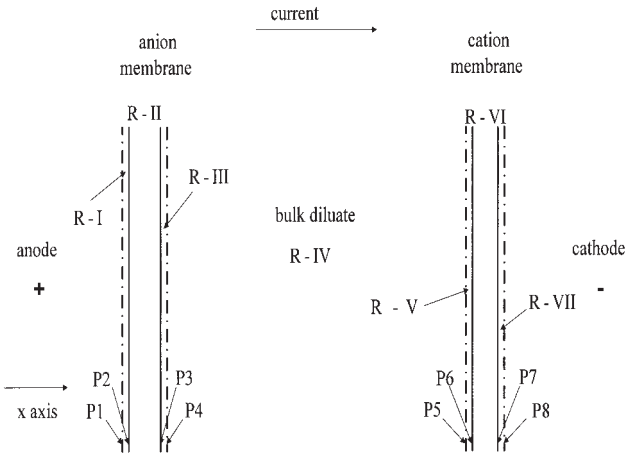

Figure 3. Schematic of regions in a cell pair.

The initial condition is as follows:

$$C_i(j) = C^0_{h,i}, \quad h = \text{C, D} \;\; j = \text{P1, P4, P5, and P8} \tag{12}$$

The boundary conditions at $x =$ P2, P3, P6, and P7 are given by:

$$J_{h,i} = \bar{J}_i \quad \text{for } h = \text{C, D;} \quad i = 2; x = \text{P2, P3}$$
$$J_{h,i} = 0 \quad \text{for } h = \text{C, D;} \quad i = 1; x = \text{P2, P3}$$

$$J_{h,i} = \bar{J}_i \quad \text{for } h = \text{D, C;} \quad i = 1; x = \text{P6, P7}$$
$$J_{h,i} = 0 \quad \text{for } h = \text{D, C;} \quad i = 2; x = \text{P6, P7}$$

$$K_{h,i} = \frac{\bar{C}_i}{C_i(x)} = \frac{Q_{\text{AM or CM}}}{|n_i| C_i(x)} \quad \text{for } h = \text{C, D;} \quad i = 1, 2; \quad x = \text{P2, P3, P6, P7} \tag{13}$$

The initial conditions, Eq. (12), specify concentrations for ionic bulk dilute and concentrate. The electric potential at $x =$ P1 is set to zero. We choose the value for the electric potential because only potential differences are meaningful.[13] The boundary conditions in Eq. (13) use fluxes at the membrane–solution interface of each compartment to show charge transfer of the ionic species.[14–16]

We solve Eq. (9) by a finite-difference method with the Newton–Raphson iterative technique under restrictions of Eqs. (12) and (13) and the electroneutrality condition. Physical properties and parameters are listed in Table 1.

Table 1. Physical properties and parameters used in simulations.

Solution phase	
K^+ diffusion coefficient ($m^2\ sec^{-1}$)[1,20–22]	1.95×10^{-9}
Cl^- diffusion coefficient ($m^2\ sec^{-1}$)[1,20–22]	2.03×10^{-9}
Cation exchange membrane, CM-1	
K^+ diffusion coefficient ($m^2\ sec^{-1}$)[7]	1.35×10^{-10}
Membrane thickness (m)[7]	1.44×10^{-4}
Ion-exchange capacity, Q_{CM} ($mol\ m^{-3}$)[7]	2.10×10^{3}
Anion exchange membrane, AM-1	
Cl^- diffusion coefficient ($m^2\ sec^{-1}$)[7]	3.27×10^{-11}
Membrane thickness (m) [7]	1.37×10^{-4}
Ion-exchange capacity, Q_{AM} ($mol\ m^{-3}$)[7]	1.52×10^{3}
Dimensions of the compartment channel	
Length of channel (m)	17.5×10^{-2}
Width of channel (m)	11.3×10^{-2}
Thickness of channel (m)	8.2×10^{-4}
Average boundary layer thickness (m)[22]	5.3×10^{-5}

Cell Pair Potential

The cell pair potential is the sum of potential gradients in the bulk region of the dilute compartment, the membrane compartments, and the boundary layers:

$$\frac{\partial\Theta}{\partial x} = \frac{\partial\Theta_{R-IV}}{\partial x} + \frac{\partial\Theta_{AM}}{\partial x} + \frac{\partial\Theta_{CM}}{\partial x} + \frac{\partial\Theta_{R-I}}{\partial x} + \frac{\partial\Theta_{R-III}}{\partial x} + \frac{\partial\Theta_{R-V}}{\partial x} + \frac{\partial\Theta_{R-VII}}{\partial x} \tag{14}$$

In the bulk region of the dilute compartment (R-IV) there is no concentration gradient; thus, the potential gradient obeys Ohm's law[8] and is given by:

$$\frac{\partial\Theta_{R-IV}}{\partial x} = -\frac{I}{\sum_i |n_i|\lambda_i C_i} \quad i = 1, 2 \tag{15}$$

where λ_i is the equivalent ion conductance. The potential difference across the membrane thickness of the cation- and the anion-exchange membrane is given by Eq. (5). The boundary layer potentials are given for R-I, R-III, R-V, and R-VII by Eq. (11).

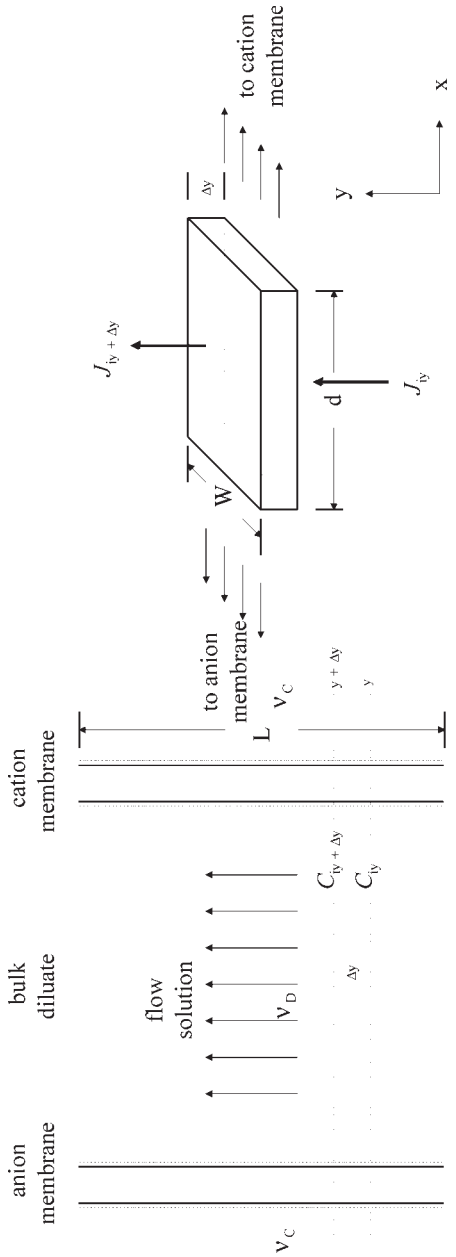

Figure 4. Two-dimensional material balance around the membranes.

Solution Phase Transport along the *y*-Axis (2-D Continuous Model)

Consider the mass flux of species *i* in the coordinate element Δy of an ED compartment (shown in Fig. 4). The concentration of species *i* is assumed to be a function of position *x* and *y*. At steady state, the balance then becomes

$$\frac{dC_{h,i}}{dy} = \pm \frac{J_{h,i}}{dv_h}; \quad h = \text{D,C boundary layer thickness } (\delta) \ll d \tag{16}$$

The compartment thickness is d; v_h, the flow solution velocities in compartments D and C; and $J_{h,i}$, the flux of species *i* in the *x* direction obtained from Eq. (9). The (+) and (−) signs apply to the concentrate (C) and the dilute (D), respectively.

In Eq. (16), diffusion and migration transport in the *y*-coordinate are negligibly small compared with convective transport in the solution phase. Based upon the Peclet number (8.0×10^6) calculations for potassium chloride with a fluid velocity of 0.05 m sec^{-1}, we assume that the diffusion transport on the *y*-axis is negligible (concentration gradients are negligible in comparison with concentration gradients along the *x*-axis).[17,18]

The initial conditions at the inlet of each compartment ($h = \text{D,C}$) are:

$$y = 0 \quad C_{h,i}(x) = C_{h,i}(x)|_{\text{in}}; \quad x = \text{P1, P4, P5, P8} \tag{17}$$

Batch Model

Let us consider the batch process in which the dilute (feed) and the concentrate (product) solutions are circulating with pumps between the ED stack and the tanks.[19] Assuming a pseudo-steady state approximation in the cell pair and perfect mixing in the solution of the tanks,[7] one can write an overall balance in the tank for the transport of the salt solution, KCl, and water (w) as follows:

Salt balance

$$\frac{d(V_r C_{r,\text{s}})}{dt} = \pm J_{h,\text{s}}\, S_{\text{m}}\, N; \quad r = \text{DT, CT} \tag{18}$$

Initial condition

$$t = 0 \quad \begin{aligned} C_{r,\text{s}} &= C_{r,\text{s}}|_{t=0}; \quad r = \text{DT, CT} \\ V_r &= V_r|_{t=0} \end{aligned} \tag{19}$$

Water balance

$$\frac{d(V_r C_{r,\mathrm{w}})}{dt} = \pm J_{h,\mathrm{s}}\, S_{\mathrm{m}}\, N\alpha; \quad r = \mathrm{DT},\ \mathrm{CT} \tag{20}$$

where t, the time; V_r, the dilute (DT) or concentrate tank (CT) volume; $C_{r,\mathrm{s}}$ and $C_{r,\mathrm{w}}$, the salt (s) and water (w) concentrations in either the dilute or the concentrate tanks; and S_{m}, the effective membrane area per sheet. N is the total number of cell pairs in the electrodialysis stack, and α is an experimental value that represents the ratio of moles of water per mole of salt transported through the ion-exchange membranes from the dilute into the concentrate compartment. Finally, $J_{h,\mathrm{s}}$ is the ionic flux obtained from the steady-state equation. The signs $(-)$ and $(+)$ refer to the dilute and concentrate tank balances, respectively.

Eqs. (18) and (20) can be combined to express the water concentration, C_{w}, as a function of the solution density, ρ_r, as:

$$\frac{d(V_r \rho_r)}{dt} = \pm J_{h,\mathrm{s}} S_{\mathrm{m}} N(1+\alpha); \quad \rho_r = C_{r,\mathrm{s}} + C_{r,\mathrm{w}} \tag{21}$$

Initial condition

$$t = 0 \quad \rho_r = \rho_r|_{t=0}; \quad r = \mathrm{DT},\ \mathrm{CT} \tag{22}$$

Further rearranging of Eqs. (18) and (21) provides a salt mass fraction $X_{r,\mathrm{s}}$ relationship:

$$X_{r,\mathrm{s}}|_{t+\Delta t} = \frac{|V_r C_{r,\mathrm{s}}|_{t+\Delta t}}{|V_r \rho_r|_{t+\Delta t}} = \frac{\text{salt mass}_r|_{t+\Delta t}}{\text{solution mass}_r|_{t+\Delta t}} = \frac{C_{r,\mathrm{s}}|_{t+\Delta t}}{\rho_r|_{t+\Delta t}}; \quad r = \mathrm{DT},\ \mathrm{CT} \tag{23}$$

Eqs. (18), (21), and (23) represent six equations with eight variables: $C_{\mathrm{DT,s}}$, $C_{\mathrm{CT,s}}$, V_{DT}, V_{CT}, $X_{\mathrm{DT,s}}$, $X_{\mathrm{CT,s}}$, ρ_{DT}, and ρ_{CT}. To solve these material-balance equations, two additional relations are needed. These relations are provided by the salt mass fraction $X_{r,\mathrm{s}}$, which is also related to its density ρ_r. The following correlation was derived and rearranged by Treybal:[17]

$$\rho_r = 6772.1 X_{r,\mathrm{s}}|_{t+\Delta t} + 995402;$$
$$r = \mathrm{DT},\ \mathrm{CT};\ \mathrm{s} = \mathrm{KCl};\ \rho_r\ (\text{gram of KCl m}^{-3}\text{solution});$$
$$X_{r,\mathrm{s}}\ (\text{gram KCl per 100 gram solution}); \tag{24}$$

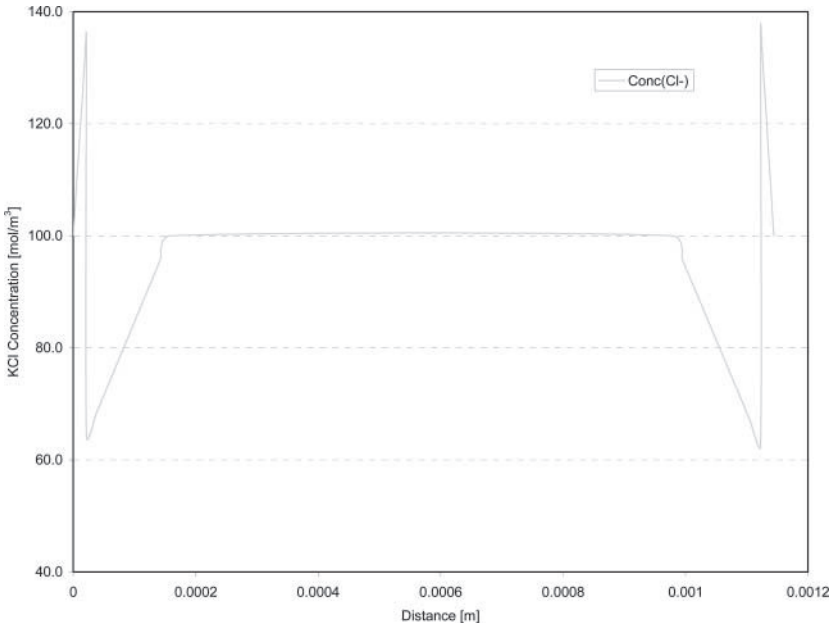

Figure 5. Typical KCl concentration profile along an ED cell compartment.

RESULTS AND DISCUSSION

Steady-State Model Prediction Along *x*-Axis Near Ion-Exchange Membranes

Dilute Concentration Effect

Five theoretical simulations were conducted for several KCl dilute concentrations. For all five simulations (100, 200, 300, 400, and 500 mol m^{-3}), the current density was 650 A m^{-2} and the initial KCl concentrate concentration was 100 mol m^{-3}. A typical KCl concentration profile along the compartment cell is shown in Fig. 5. This profile shows a sharp decrease of the KCl concentration in the dilute compartment near the boundary layers and an increase in the concentrate compartment near the membrane side. In the boundary layer of the dilute compartment, the ion concentration is depleted by the contribution of diffusion and electromigration as the ion transport from the dilute to the concentrate compartment. On the other side of the membrane in the concentrate compartment, the ion concentration near the membrane surface is high because of the high ion-exchange capacity of the

membrane. The KCl concentration in the concentrate compartment reduces gradually with position as the ions move away from the membrane and are mixed into the bulk solution.

Simulation results in Table 2 show that toward the anion-exchange membrane in the boundary layer region (R-III), the Cl^- flux is $6.74 \times 10^{-3}\,mol\,m^{-2}\,sec^{-1}$ and zero for K^+. Similarly, toward the cation-exchange membrane in the boundary layer region (R-V), the K^+ flux is $6.74 \times 10^{-3}\,mol\,m^{-2}\,sec^{-1}$ and zero for Cl^-. In regions (R-III) and (R-V), the flux of K^+ and the flux of Cl^- are zero because they are the co-ions of the cation- and the anion-exchange membranes, respectively. For all these simulations, the current density remains constant.

As the KCl dilute concentration increases from 100 to $500\,mol\,m^{-3}$, the cell voltage drop, $\Delta\Theta$, decreases from 1.42 to 0.98 V (Table 3). The cell voltage decreases mainly because of an increase in the dilute bulk conductivity, which decreases the dilute bulk drop ($\Delta\Theta_{R\text{-}IV}$) and the voltage drop in Regions III and V. At the lowest KCl dilute concentration, the total dilute drop [$\sum (\Delta\Theta_{R\text{-}III} + \Delta\Theta_{R\text{-}IV} + \Delta\Theta_{R\text{-}V})$] accounts for 36% of the cell drop. At the highest KCl dilute concentration, this value is reduced to 7%. When the KCl dilute concentration doubles, the dilute bulk drop decreases by approximately one-half.

In these simulations, the anion- ($\Delta\Theta_{AM}$) and the cation-exchange ($\Delta\Theta_{CM}$) membrane drops remain unchanged for a constant current density. The voltage drop of the anion membrane is five times higher than that of the cation membrane. The anion membrane drop is higher because of a lower counter ion diffusivity and lower ion-exchange membrane capacity. The ion-exchange membrane drop is proportional to the current and the membrane resistance. For each membrane, the resistance is inversely proportional to the counter ion diffusivity of the membrane and its ion-exchange membrane capacity. For these simulations, the AM-1 membrane capacity ($1.52 \times 10^3\,mol\,m^{-3}$) and the chloride diffusivity ($3.27 \times 10^{-11}\,m^2\,sec^{-1}$) through the anion membrane are lower than that of the CM-1 membrane capacity ($2.10 \times 10^3\,mol\,m^{-3}$) and the potassium diffusivity ($1.35 \times 10^{-10}\,m^2\,sec^{-1}$) through the cation-exchange membrane.

At dilute concentrations higher than $200\,mol\,m^{-3}$, the membrane voltage drop ($\Delta\Theta_{AM}$ and $\Delta\Theta_{CM}$) accounts for more than 50% of the cell voltage drop. This contribution to the cell voltage drop increases with increasing the KCl dilute concentration, which decreases the resistance in both the dilute boundary layers (R-III and R-V) and the dilute bulk (R-IV). For all these simulations, the KCl concentration in the concentrate side is constant.

Current Density Variation

Simulations were done at three current densities (100, 250, and $500\,A\,m^{-2}$). The initial KCl concentration in the dilute and the concentrate

Table 2. Simulation fluxes (mol $m^{-2} sec^{-1}$) obtained for K^+ and Cl^- ionic species in boundary layers (R-III and R-V) with several initial KCl dilute concentrations (DC in mol m^{-3}). The overall flux includes diffusion and migration contributions. The initial KCl concentrate concentration and current density were 100 mol m^{-3} and 650 A m^{-2}, respectively.

Region	Species	Flux	DC 100×10^3	DC 200×10^3	DC 300×10^3	DC 400×10^3	DC 500×10^3
R-III	K^+	Overall	0.00	0.00	0.00	0.00	0.00
	Cl^-	Overall	−6.74	−6.74	−6.74	−6.74	−6.74
R-V	K^+	Overall	6.74	6.74	6.74	6.74	6.74
	Cl^-	Overall	0.00	0.00	0.00	0.00	0.00

Note: The minus sign refers to a flux value in opposite direction of the electrical current.

Table 3. Simulation voltage drop values obtained for different KCl dilute concentrations, DC. The initial KCl concentrate concentration and current density were 100 mol m^{-3} and 650 A m^{-2}, respectively.

DC (mol m^{-3})	$\Delta\Theta_{R\text{-}I}$ (V)	$\Delta\Theta_{AM}$ (V)	$\Delta\Theta_{R\text{-}III}$ (V)	$\Delta\Theta_{R\text{-}IV}$ (V)	$\Delta\Theta_{R\text{-}V}$ (V)	$\Delta\Theta_{CM}$ (V)	$\Delta\Theta_{R\text{-}VII}$ (V)	$\Delta\Theta$ (V)
100	0.012	0.477	0.024	0.310	0.173	0.088	0.022	1.416
200	0.012	0.477	0.011	0.155	0.021	0.088	0.022	1.096
300	0.012	0.477	0.008	0.103	0.011	0.088	0.022	1.031
400	0.012	0.477	0.006	0.077	0.008	0.088	0.022	1.000
500	0.012	0.477	0.004	0.062	0.006	0.088	0.022	0.981

was 100 mol m^{-3}. A direct correlation of the current density with the flux was observed for these simulations (Table 4). At the highest ionic flux (5.18×10^{-3} mol m^{-2} sec^{-1}), where the current density is 500 A m^{-2}, the K^+ and Cl^- species reach (by diffusion and migration) the cation- and the anion- exchange membrane surfaces faster than at the current densities of 100 and 250 A m^{-2}. The overall K^+ flux contribution is not shown in Table 4. At the highest current density, the Cl^- membrane surface concentration is 26 mol m^{-3}. At the lowest current density, 100 A m^{-2}, the ionic flux is the lowest (1.04×10^{-3} mol m^{-2} sec^{-1}). A lower ionic flux indicates that ionic species reach the anion exchange membrane at a lower rate, resulting in a higher dilute surface concentration (94 mol m^{-3}).

Increasing the current density increases the cell voltage. For all these current densities, the anion membrane drop, the bulk dilute drop, and the concentrate drop collectively account for more than 82% of the cell voltage, where 36% of the cell voltage corresponds to the anion membrane drop (data not shown).

Concentrate Concentration Effect

The effect of the concentrate concentration was studied by maintaining the current density at 650 A m^{-2} and the dilute concentration at 100 mol m^{-3}. Results show that an increase in the concentrate concentration causes the partition coefficient at the membrane surfaces on the concentrate side to decrease.

The profiles of the ion partition coefficient on the concentrate side of the anion and the cation-exchange membrane surface are shown in Fig. 6. Both ion partition coefficients decrease as the KCl concentration increases. The partition coefficient is the ratio of the membrane ion exchange capacity to its counter ion membrane surface concentration. As the KCl concentration increases, the counter ion surface concentration increases in the concentrate side. At any given KCl concentration, the ion partition coefficient in the cation

Table 4. Effect of current density on the overall flux, cell voltage, and membrane surface concentration.

Current density (A m^{-2})	Overall Cl^- flux near cation membrane (mol m^{-2} sec^{-1})	Cell voltage (V)	Cl^- anion membrane surface concentration (mol m^{-3})
100	1.04×10^{-3}	0.196	94
250	2.59×10^{-3}	0.493	69
500	5.18×10^{-3}	1.011	26

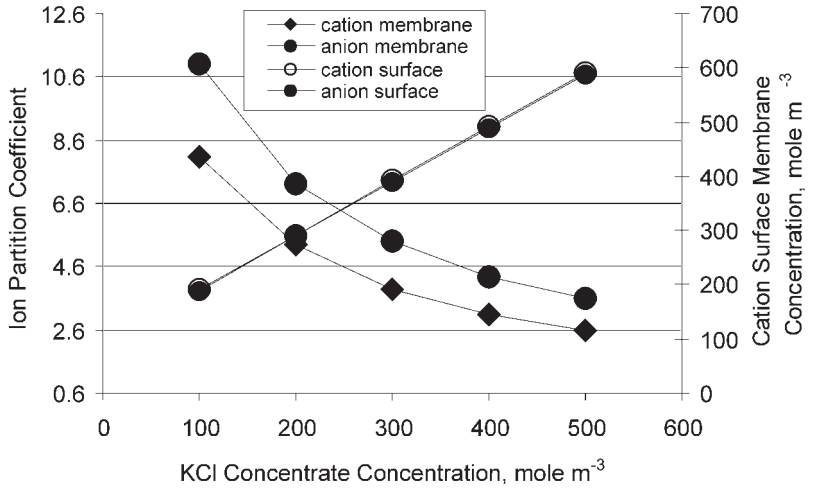

Figure 6. Variation of the ion partition coefficient and surface membrane concentration with KCl concentration.

membrane is larger than in the anion membrane. In both ion-exchange membranes, the counter ion concentration is proportional to their ion-exchange capacity, with the cation membrane being the largest. Also, concentrations at both the membrane surfaces on the concentrate side are comparable. This fact explains the greater partition coefficient values of K^+ in the cation membrane side. For all five simulations on the dilute side, the ion partition coefficients remained constant because the initial KCl dilute concentration was unchanged.

Steady-State Model Prediction Along the *x*- and the *y*-Axes

The effect of three superficial velocities (0.02, 0.05, and 0.15 m sec^{-1}) on concentration, voltage drops, and flux was studied. These steady-state simulations were carried out for a current density of 500 A m^{-2}. The initial KCl concentration in the dilute and the concentrate compartments was 100 mol m^{-3}.

Results show greater variation of the potassium chloride concentration along the *x*-axis (perpendicular to the flow) than that of the *y*-axis (parallel to the flow). Concentration changes along the *x*-axis are larger ($> 50\%$) because of the ionic flux, which is favored by the electric field and a low superficial velocity. Along the *y*-axis, the variation of the concentration is well below 2%. An increase in the superficial velocity decreases the contact time of the fluid with the membrane surfaces, reducing the boundary layer

thickness. No significant cell voltage changes are observed with variations in the superficial velocity along the compartment height.

Batch Simulation

Three batch simulations at current densities of 700, 500, and 300 A m^{-2} were run for a KCl solution. Each batch simulation was run for a total of 10 cell pairs with AM-1 and CM-1 membranes. The effective membrane per sheet was 0.02 m^{-2}. The initial KCl concentration was 30 g L^{-1} in the dilute and 5 g L^{-1} in the concentrate. The initial dilute and concentrate volume of these simulations were 10 and 5 L, respectively.

Results show that an increase in the current density leads to a decrease in the time required to obtain the same degree of desalting. Faster desalination is achieved at the highest current density of 700 A m^{-2}. The time required for obtaining a 50% desalting of the initial KCl mixture in the dilute tank at a current density of 300, 500, and 700 A m^{-2} are 3300, 2000, and 1450 sec, respectively. The KCl concentration and volume increased in the concentrate tank. The primary explanation for volume changes during desalting by batch ED is ion hydration. Computational results show an overall decrease in the KCl concentration in the dilute tank (Fig. 7) and an increase in the concentrate tank (Fig. 8).

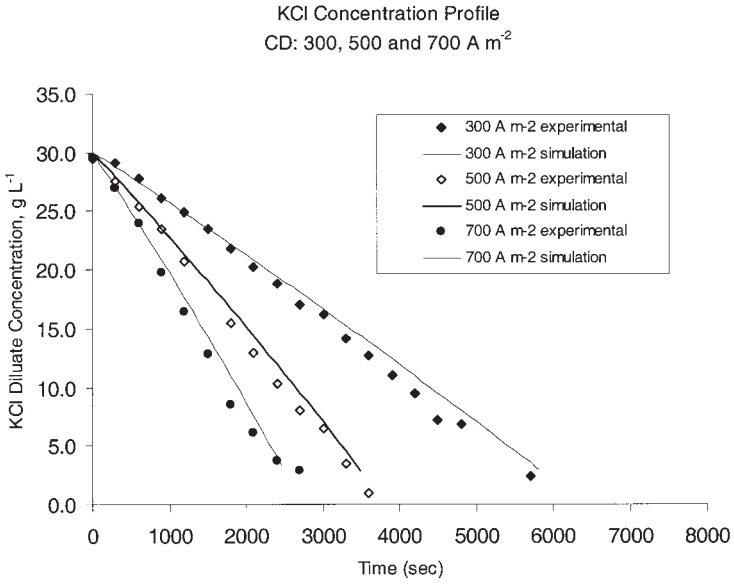

Figure 7. Potassium chloride concentration profiles in the dilute tank.

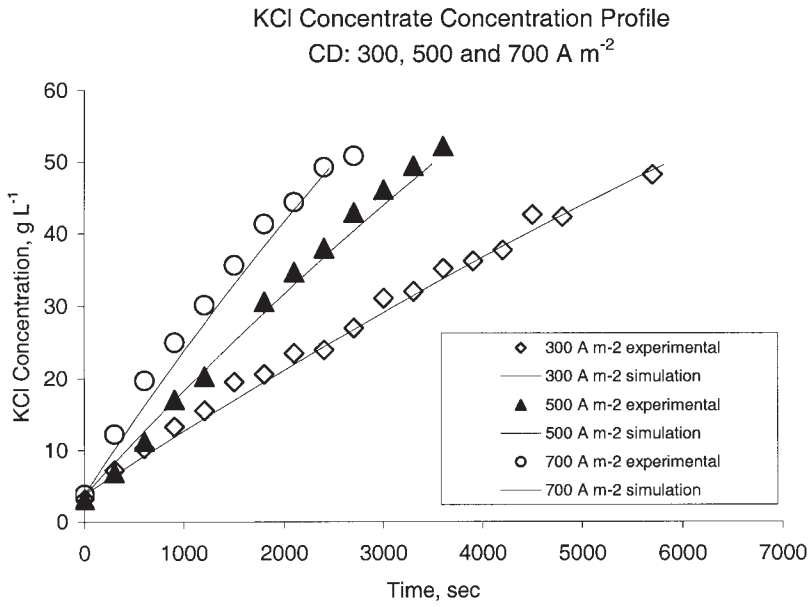

Figure 8. Potassium chloride concentration profiles in the concentrate tank.

CONCLUSIONS

All three models—one-dimensional continuous, two-dimensional continuous, and batch—were validated experimentally. Computational simulations and batch experimental runs were conducted under similar conditions and show a good fit. One- and two-dimensional steady-state models were used as the basis of the batch model.

The ionic surface concentration in both membranes of the dilute compartment was affected by two parameters: flow rate and current density. A high flow rate causes a small boundary layer thickness and a high ionic surface concentration. When the current density is high, the ionic flux is also high, and the ionic surface concentration is low.

Also, in the dilute compartment, it is found that concentration changes along the x-axis are greater than along the y-axis because the ionic flux along the x-axis is greater and is in the direction of the current.

In simulations where the KCl dilute concentration ranges from 200 to 500 mol m^{-3} with a constant concentrate concentration, it is found that the dilute voltage drop accounts for more than 36% of the total voltage drop. This value is reduced to 7% at the highest dilute concentration. At a KCl

concentration higher than 200 mol m^{-3}, contributions of both ion-exchange membrane voltages contribute more than 50% of the total cell voltage.

NOMENCLATURE

$C^0_{R,i}$	Initial concentration of either dilute or concentrated compartment (mol m^{-3})
$C_{R,i}$	Concentration of either dilute or concentrated compartment (mol m^{-3})
C_i	Concentration of species i (mol m^{-3})
$\bar{C}_i$	Concentration of species i in the membrane (mol m^{-3})
$C_{r,s}$	Concentration of salt in dilute and concentrate tanks (mol m^{-3})
$C_{r,w}$	Concentration of water in dilute and concentrate tanks (mol m^{-3})
d	Compartment thickness (m)
d_e	Hydraulic diameter (m)
D_s	Salt solution diffusion coefficient ($m^2\,sec^{-1}$)
D_i	Diffusion coefficient of species i in solution ($m^2\,sec^{-1}$)
$\bar{D}_i$	Diffusion coefficient of species i in solution ($m^2\,sec^{-1}$)
F	Faraday's constant
I	Current density in the solution (A m^{-2})
$\bar{I}$	Current density in the ion-exchange membrane (A m^{-2})
i	Species 1 and 2
J_i	Flux of species i (mol m^{-2} sec)
$J_{h,s}$	Ionic flux at steady state condition
$\bar{J}_i$	Mass flux of each ion in the membrane (mol m^{-2} sec)
j	Electrodialysis stack position P1, P4, P5, and P8
h	Dilute (D) or concentrate (C) compartment (m)
K	Partition coefficient
N	Total number of cell pairs
n_i	Valence of species i
Pe	Peclet number
Q_{AM}	Capacities of anion-exchange membrane (mol m^{-3})
Q_{CM}	Capacities of cation-exchange membrane (mol m^{-3})
R	Gas constant number (J K mol^{-1})
R_i	Production rate of ion i by chemical reaction
Re	Reynolds number
r	Dilute (DT) and concentrated tank (CT) (m^3)
Sc	Schmidt number
S_m	Effective membrane area per sheet (m^2)

s	Salt species
T	Temperature (K)
t	Time (sec)
u_i	Mobility of species i, ($cm^2\,mol\,J^{-1}\,sec^{-1}$)
V_r	Dilute and concentrate tank volume (m^3)
w	Water species
$X_{r,s}$	Salt mass fraction
x	x coordinate
y	y coordinate
$\Theta_{R\text{-}IV}$	Dilute compartment bulk region potential (V)
$\Theta_{R\text{-}I}$, $\Theta_{R\text{-}III}$, $\Theta_{R\text{-}V}$, $\Theta_{R\text{-}VII}$	Boundary layer potential (V)
Θ_{AM}	Anion membrane potential
Θ_{CM}	Anion and cation membrane potential
α	Ratio of moles of water per mole of salt transported through the ion-exchange membrane
k_L	Mass transfer coefficient ($m\,sec^{-1}$)
ρ_r	Solution density ($g\,m^{-3}$)
v	Fluid velocity ($m^3\,sec^{-1}$)
v_h	Flow solution velocity in dilute and concentrate compartment ($m^3\,sec^{-1}$)
$\nabla\Theta$	Potential difference of the membrane (V)
$\bar{\Theta}$	Potential in the membrane
Δt	Time step change (sec)
λ_i	Equivalent ion conductance ($cm^2\,ohm^{-1}\,equiv.^{-1}$)

ACKNOWLEDGMENTS

This work was supported by the U.S. Department of Energy, Assistant Secretary for Energy Efficiency and Renewable Energy, under contract W-31-109-ENG-38. Discussions and contributions by S.-P. Tsai and S. J. Parulekar are gratefully acknowledged.

REFERENCES

1. Helfferich, F. *Ion Exchange,*, 1st Ed.; McGraw-Hill: New York, 1962.
2. Strathmann, H. *Membrane Handbook*; Ho, W.S.W., Sirkar, K.K., Eds.; Van Nostrand Reinhold: New York, 1992; 219–262, Chap. 16–20.
3. Kojima, T.; Furusaki, S.; Saito, K. A fundamental study on recovery of copper with a cation exchange membrane. Can. J. Chem. Eng. **1982**, *60*, 650.

4. Inenaga, K.; Yoshida, N. Effect of an unstirred layer on ion transport through a membrane. J. Membr. Sci. **1980**, *6*, 271.
5. Verbrugge, M.W.; Hill, R.F. Ion and solvent transport in ion-exchange membranes, I: a macrohomogeneous mathematical model. J. Electrochem. Soc. **1990**, *137*, 886.
6. Chatchupong, T.; Murphy, R.J. Model of electrodialysis process associated with organic adsorption. J. Environ. Eng. **1996**, *122*, 154.
7. Sato, K.; Yonemoto, T.; Tadaki, T. Modeling of ionic transport in neutralization dialytic deionization. J. Chem. Eng. Jap. **1993**, *26*, 68.
8. Prentice, G. *Electrochemical Engineering Principles*; Prentice Hall: Englewood Cliffs, New Jersey, 1991.
9. Sato, K.; Fukuhara, C.; Yonemoto, T.; Tadaki, T. Ionic transport in a continuous Donnan dialyzer with parallel plate channel and an agitated tank. J. Chem. Eng. Jap. **1991**, *24*, 81.
10. Kikuchi, K.; Gotoh, T.; Takahashi, H.; Higashino, S.; Dranoff, J.S. Separation of aminoacids by electrodialysis with ion-exchange membranes. J. Chem. Eng. Jap. **1995**, *28*, 103.
11. Goodridge, F.; Scott, K. *A Guide to the Design of Electrolytic Plant*; Plenum Press: New York, 1995.
12. Newman, J.S. *Electrochemical Systems*, 2nd Ed.; Prentice Hall: Englewood Cliffs, New Jersey, 1991.
13. Kuz'minykh, V.A.; Grigorchuck, O.V.; Shaposhnik, V.A. Hydrodynamic model of electrodialysis with ion-exchange membranes of different selectivity. Russ. J. Electrochem. **1994**, *30*, 1001.
14. Gnusin, N.P.; Kononenko, N.A.; Parshikov, S.B. Electrodiffusion through an inhomogeneous ion-exchange membrane with adjacent diffusion layers. Russ. J. Electrochem. **1994**, *30*, 28.
15. Huang, T.-C.; Lin, Y.-K. The interdiffusion of counterions in a cation-exchange membrane with metal chelation in solution phase. J. Chem. Eng. Jap. **1987**, *20*, 511.
16. Nikonenko, V.; Zabolotsky, V.; Larchet, C.; Auclair, B.; Pourcelly, G. Mathematical description of ion transport in membrane systems. Desalination **2002**, *147*, 369.
17. Treybal, R.E. *Mass Transfer Operations*, 3rd Ed.; McGraw-Hill: New York, 1980.
18. Green, D.W. *Perry's Chemical Engineers' Handbook*, 6th Ed.; McGraw-Hill: New York, 1984.
19. Moon, P.J.; Parulekar, S.J.; Tsai, S.-P. Competitive anion transport in desalting of mixtures of organic acids by batch electrodialysis. J. Membr. Sci. **1998**, *141*, 75.

20. Horvath, A.L. *Handbook of Aqueous Electrolyte Solutions: Physical Properties, Estimation, and Correlation Methods*; John Wiley & Sons: New York, 1985.
21. Dean, A. *Lange's Handbook of Chemistry*, 14th Ed.; McGraw-Hill: New York, 1985.
22. Fares, A.; Sandeaux, J.; Sandeaux, R.; Gavach, C. Transport properties of electrodialysis membranes in the presence of arginine, II: competition between the electrotransport of organic and inorganic ions through a cation exchange membrane in an aqueous solution of arginine chlorhydrate and sodium chloride. J. Membr. Sci. **1994**, *89*, 83.